arXiv:cond-mat/0204358 v1 17 Apr 2002

Cohesion and Stability of Metal Nanowires: A Quantum Chaos Approach*

C. A. Stafford[1], F. Kassubek[2], and Hermann Grabert[2]

[1] Department of Physics, University of Arizona
1118 E. 4th Street, Tucson, AZ 85721, USA
[2] Fakultät für Physik, Albert-Ludwigs-Universität
Hermann-Herder-Straße 3, D-79104 Freiburg, Germany

Abstract. A remarkably quantitative understanding of the electrical and mechanical properties of metal wires with a thickness on the scale of a nanometer has been obtained within the free-electron model using semiclassical techniques. Convergent trace formulas for the density of states and cohesive force of a narrow constriction in an electron gas, whose classical motion is either chaotic or integrable, are derived. Mode quantization in a metallic point contact or nanowire leads to universal oscillations in its cohesive force, whose amplitude depends only on a dimensionless quantum parameter describing the crossover from chaotic to integrable motion, and is of order 1nN, in agreement with experiments on gold nanowires. A linear stability analysis shows that the classical instability of a long wire under surface tension can be completely suppressed by quantum effects, leading to stable cylindrical configurations whose electrical conductance is a magic number 1, 3, 5, 6,... times $2e^2/h$, in accord with recent results on alkali metal nanowires.

1 Introduction

In 1971, Gutzwiller's trace formula [1] expressing the quantum density of states of a classically chaotic system as a Feynman sum over classical periodic orbits gave birth to the field of quantum chaos. In the subsequent decades, the trace formula was generalized, and applied to a wide variety of physical systems [2,3]. Of particular interest here are trace formulas for systems with continuous symmetries [4,5] and broken symmetries [6,7]. One of the most important successes of this semiclassical approach has been the description of shell effects in finite fermion systems [3,8]. In this article, we discuss the application [9,10,11,12] of trace formulas to describe quantum-size effects in a particular class of open quantum systems: metallic nanocontacts and nanowires.

In the past eight years, experimental research on atomically-thin metal wires has burgeoned [13,14,15,16,17,18,19,20,21,22]. In a seminal experiment [14] carried out in 1995, Rubio, Agraït and Vieira simultaneously measured the electrical conductance and cohesive force of an atomic-scale gold contact as it formed and ruptured (see Fig. 1). They observed steps of order

* B. Kramer (Ed.): Adv. in Solid State Phys. **41**, 497-511 (2001)

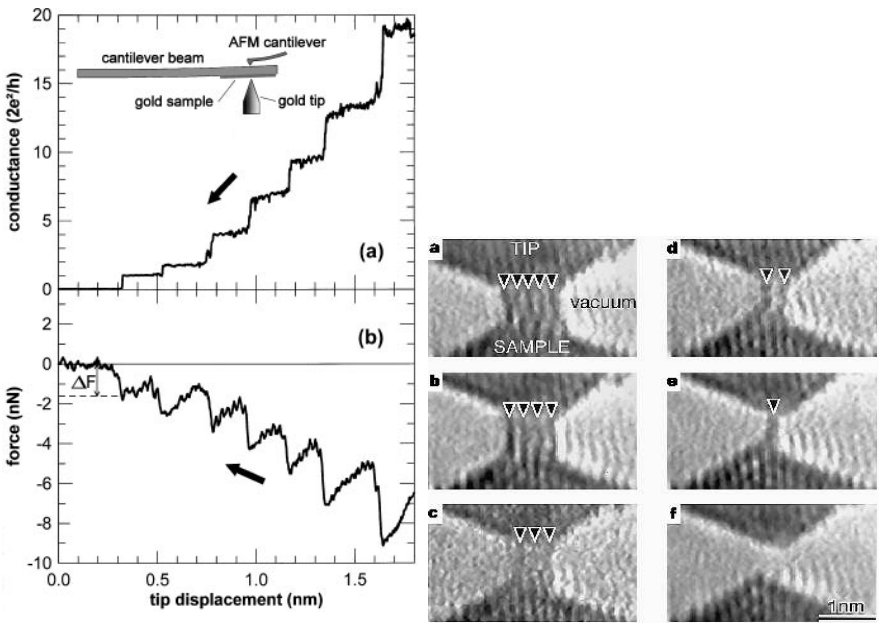

Fig. 1. Left: Simultaneous measurements of (**a**) the conductance and (**b**) the cohesive force of a gold nanowire during elongation at room temperature, from Ref. [14]. Right: Transmission electron micrographs of an atomic-scale gold contact breaking, from Ref. [19]. The measured electrical conductance of the contact is (**d**) $G \simeq 2G_0$, (**e**) $G \simeq G_0$

$G_0 = 2e^2/h$ in the conductance, which were synchronized with a sawtooth structure with an amplitude of order 1nN in the force. Similar results were obtained independently by Stalder and Dürig [15]. For comparison, electron micrographs by Ohnishi *et al.* [19] illustrating the atomic-scale structure of a gold nanocontact breaking are also shown in Fig. 1.

Conductance steps of size G_0 were first observed in quantum point contacts (QPCs) fabricated in semiconductor heterostructures [23], and are a rather universal phenomenon in metal nanowires [13], even being found in contacts formed in liquid metals [17]. The precision of conductance quantization in metal nanocontacts is poorer than that in semiconductor QPCs due to their inherently rough structure on the scale of the Fermi wavelength λ_F, which causes backscattering [24], and due to the imperfect hybridization of the atomic orbitals in the contact, especially for multivalent atoms [18]. As we shall see in the following, the sawtooth structure in the cohesive force can be considered a mechanical analogue of conductance quantization [25].

A remarkable feature of metal nanowires is the fact that they are stable at all. Fig. 2 shows electron micrographs by Kondo and Takayanagi [16] illustrating the formation of a gold nanowire. Under electron beam irradiation,

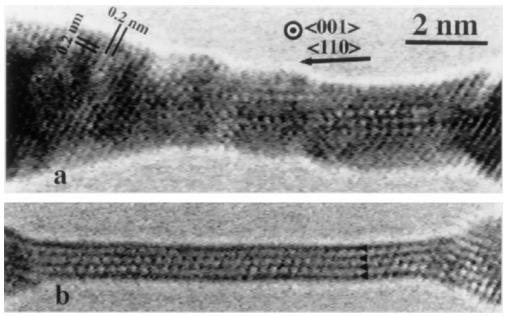

Fig. 2. Transmission electron micrographs showing the formation of a gold nanowire, from Ref. [16]: (**a**) an image of Au(001) film with closely spaced nanoholes, the initial stage of the nanowire; (**b**) a nanowire four atoms in diameter, resulting from further electron-beam irradiation

the wire becomes ever thinner, until it is but four atoms in diameter. Almost all of the atoms are at the surface, with small coordination numbers. The surface energy of such a structure is enormous, yet it is observed to form spontaneously, and to persist almost indefinitely. Even wires one atom thick, such as that shown in Fig. 1(e), are found to be stable for days at a time [19,20]. Naively, such structures might be expected to break apart due to surface tension [26,27,28], but we shall show that quantum-size effects can stabilize arbitrarily long nanowires [12].

2 Free electron model

We investigate the simplest possible model [25,29] for a metal nanowire: a free (conduction) electron gas confined within the wire by Dirichlet boundary conditions. A nanowire is an open quantum system, and so is treated most naturally in terms of the electronic scattering matrix S. The Landauer formula [30,31] expressing the electrical conductance in terms of the submatrix S_{12} describing transmission through the wire is

$$G = \frac{2e^2}{h} \int dE \frac{-\partial f(E)}{\partial E} \mathrm{Tr} \left\{ S_{12}^\dagger(E) S_{12}(E) \right\}, \tag{1}$$

where $f(E)$ is the Fermi-Dirac distribution function. The conductance of a metal nanocontact was calculated exactly in this model by Torres *et al.* [32]. The appropriate thermodynamic potential to describe the energetics of such an open system is the grand canonical potential Ω, whose derivative with respect to elongation gives the cohesive force F:

$$\Omega = -\frac{1}{\beta} \int dE\, g(E) \ln \left(1 + e^{-\beta(E-\mu)} \right), \qquad F = -\frac{\partial \Omega}{\partial L}. \tag{2}$$

Here β is the inverse temperature, μ is the chemical potential of electrons injected into the nanowire from the macroscopic electrodes, and $g(E)$ is the

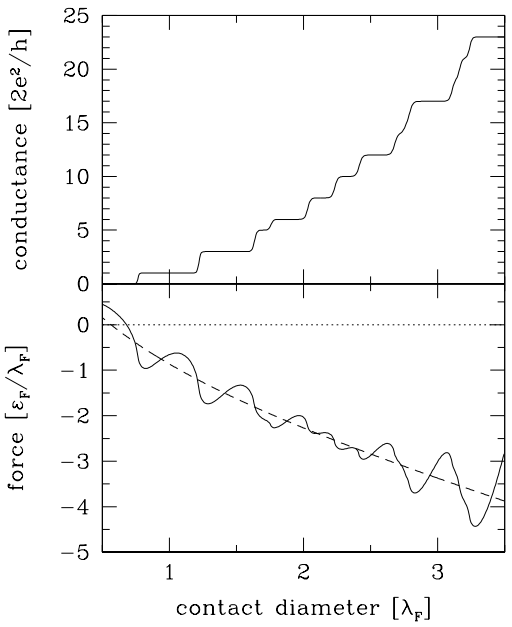

Fig. 3. Electrical conductance and cohesive force of a nanowire, modeled as a narrow neck in a free-electron gas, calculated from Eqs. (1)–(3) at zero temperature. The S-matrix was calculated using the adiabatic and WKB approximations, following Ref. [25]. For comparison, the contribution to the force from the surface tension and curvature energy is shown as a dashed line. Note that $\varepsilon_F/\lambda_F = 1.7$nN in gold

electronic density of states (DOS) of the nanowire. The DOS of an open system may be expressed in terms of the scattering matrix as [33]

$$g(E) = \frac{1}{2\pi i}\mathrm{Tr}\left\{ S^{\dagger}(E)\frac{\partial S}{\partial E} - \mathrm{H.c.}\right\}. \tag{3}$$

This formula is also known as the Wigner delay. Note that in Eqs. (1) and (3), a factor of 2 for spin degeneracy has been included. Thus, once the electronic scattering problem for the nanowire is solved, both the conductance and force can be readily calculated [25,29,24], as shown in Fig. 3. One sees that there is an almost quantitative agreement with the experimental results shown in Fig. 1: for example, the force necessary to break the last conducting channel is approximately ε_F/λ_F (=1.7nN in gold), where ε_F is the Fermi energy.

3 Weyl expansion

In order to separate out the mesoscopic sawtooth structure in the force, associated with the opening of individual conductance channels, from the overall (macroscopic) trend of the contact to become stronger as its diameter increases, it is useful to perform a systematic semiclassical expansion [2,3] of the DOS, $g(E) = \bar{g}(E) + \delta g(E)$, where $\bar{g}$ is a smooth average term, referred to as the Weyl contribution, and $\delta g(E)$ is an oscillatory term, whose average

is zero. For the free electron model with Dirichlet boundary conditions, the Weyl term is [3]

$$\bar{g}(E) = E^{-1}\left(\frac{k_E^3 V}{2\pi^2} - \frac{k_E^2 A}{8\pi} + \frac{k_E K}{6\pi^2}\right), \tag{4}$$

where $k_E = \sqrt{2mE}/\hbar$, V is the volume of the wire, A its surface area, and K the integrated mean curvature of its surface. Inserting Eq. (4) into Eq. (2), one finds the following semiclassical expansion at zero temperature:

$$\frac{\Omega}{\varepsilon_F} = -\frac{2k_F^3 V}{15\pi^2} + \frac{k_F^2 A}{16\pi} - \frac{2k_F K}{9\pi^2} + \frac{\delta\Omega}{\varepsilon_F}. \tag{5}$$

One can show [10] that interaction effects are higher order in $\hbar$. In the same spirit, a semiclassical expansion for the conductance $G = (2e^2/h)G_S + \delta G$ may be derived, where the corrected Sharvin conductance is [32]

$$G_S = \left(\frac{k_F D^*}{4}\right)^2 \left(1 - \frac{4}{k_F D^*}\right). \tag{6}$$

Here D^* is the narrowest diameter of the nanowire.

When the wire is elongated, the atoms rearrange themselves, but the volume per atom remains essentially constant [10,29]. Thus, when differentiating Eq. (5) to calculate F, the first term on the r.h.s. gives zero:

$$F = -\frac{\partial\Omega}{\partial L} = -\sigma\frac{\partial A}{\partial L} + \gamma\frac{\partial K}{\partial L} + \delta F. \tag{7}$$

The cohesive force is given by surface tension plus a small curvature correction (the sum of which is indicated by a dashed curve in Fig. 3), combined with an oscillatory quantum term.

4 Trace formulas

The oscillatory contribution $\delta g(E)$ to the DOS may be approximated as a Feynman sum over classical periodic orbits à la Gutzwiller [2,3]. Since we are interested in modeling nanowires which may possess axial and/or translational symmetries, however, we can not in general utilize Gutzwiller's original trace formula [1], which describes systems whose periodic orbits are isolated, but must instead employ a generalization due to Creagh and Littlejohn, describing a system with an f-dimensional Abelian symmetry [5]:

$$\delta g(E) = \frac{2}{\pi\hbar}\frac{1}{(2\pi\hbar)^{f/2}}\sum_{\Gamma}\frac{T_\Gamma V_\Gamma J_\Gamma^{-1/2}}{|\det\tilde{M}_\Gamma - 1|^{1/2}}\cos\left(\frac{S_\Gamma}{\hbar} - \frac{\sigma_\Gamma\pi}{2} - \frac{f\pi}{4}\right), \tag{8}$$

where the sum runs over f-dimensional families Γ of degenerate periodic orbits, T_Γ is the period of an orbit in Γ, V_Γ is the f-dimensional volume spanned

by Γ, S_Γ is the action of the orbit, and σ_Γ is a phase shift determined by the singular points along the classical trajectory. The quantity $\tilde{M}$ is the so-called monodromy matrix, characterizing the stability of the orbit with respect to perturbations. It describes as a Poincaré map the linearized motion of small perturbations from the periodic orbit in a surface of section perpendicular to the orbit in phase space: an initial variation of momentum and position in the surface of section $(\delta r, \delta p)$ is related to the mismatch $(\delta r', \delta p')$ after one period by

$$\begin{pmatrix} \delta r' \\ \delta p' \end{pmatrix} = \tilde{M} \begin{pmatrix} \delta r \\ \delta p \end{pmatrix}. \tag{9}$$

Finally, the factor $J_\Gamma = |\det(\partial r'/\partial p)|$.

We shall also need to consider the breaking of continuous symmetries, which is elegantly described in terms of semiclassical perturbation theory [6,7], wherein the cosine in the trace formula is replaced by

$$\cos(S_\Gamma/\hbar + \theta_\Gamma) \to \mathrm{Re}\left\{ e^{i(S_\Gamma/\hbar+\theta_\Gamma)} \left\langle e^{i\Delta S_\Gamma/\hbar} \right\rangle_\Gamma \right\}, \tag{10}$$

where

$$\langle e^{i\Delta S_\Gamma/\hbar} \rangle_\Gamma = V_\Gamma^{-1} \int d\mu(g) e^{i\Delta S_\Gamma(g)/\hbar} \tag{11}$$

is an average over the measure of the broken symmetry group.

4.1 A 2D example

Before treating the three-dimensional problem of interest, it is instructive to consider a two-dimensional analogue, which is much simpler, but already contains the essential elements of the problem. To be specific, we consider a QPC whose width varies as

$$D(z) = D^* + z^2/R, \quad z \in [-L/2, L/2] \tag{12}$$

along the wire (see Fig. 4). For a finite radius of curvature R, there is only a single unstable periodic orbit (plus harmonics), which moves up and down at the narrowest point of the neck. The monodromy matrix $\tilde{M}_{\mathrm{ppo}}$ of the primitive periodic orbit is given by

$$\tilde{M}_{\mathrm{ppo}}^{1/2} = \left. \begin{pmatrix} \frac{\partial r'}{\partial r} & \frac{\partial r'}{\partial p} \\ \frac{\partial p'}{\partial r} & \frac{\partial p'}{\partial p} \end{pmatrix} \right|_{\frac{1}{2}\mathrm{ppo}} = \begin{pmatrix} 1 + D^*/R & D^*(1 + D^*/2R)/p \\ 2p/R & 1 + D^*/R \end{pmatrix}, \tag{13}$$

with eigenvalues

$$e^{\pm\chi} = 1 + D^*/R \pm \sqrt{(1 + D^*/R)^2 - 1}, \tag{14}$$

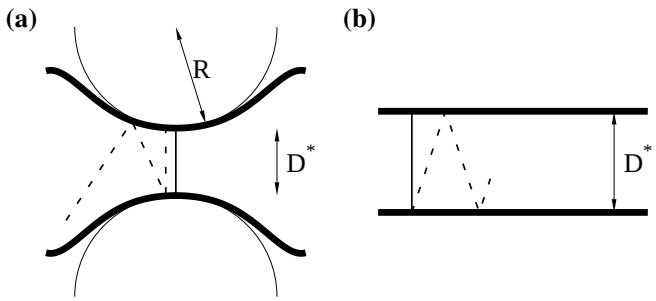

Fig. 4. Point contact (**a**) and straight wire (**b**) as limiting cases of a nanowire. The point contact is characterized by the diameter D^* and radius of curvature R of the neck. For the straight wire, $R \to \infty$. A periodic orbit is sketched with a solid line, other orbits (dotted lines) are not periodic. The classical motion in the point contact (**a**) is in general chaotic, while the straight wire (**b**) possesses integrable classical motion

2χ being the Lyapunov exponent of the primitive periodic orbit. There is no continuous symmetry present ($f = 0$), so the original Gutzwiller trace formula [1] may be used to find [10]

$$\delta g_0(E) = \frac{2mD^*}{\pi\hbar^2 k_E} \sum_{n=1}^{\infty} \frac{\cos(2nk_E D^*)}{|\sinh(n\chi)|}. \tag{15}$$

In the limit $R \to \infty$, the Lyapunov exponent $\chi \to 0$, and Eq. (15) diverges. In this limit, the wire acquires translational symmetry ($f = 1$), and Eq. (8) may be used to find

$$\frac{\delta g_1(E)}{L} = \frac{2mD^*}{\pi\hbar^2} \sum_{n=1}^{\infty} \frac{\cos(2nk_E D^* - \pi/4)}{\sqrt{\pi n k_E D^*}}. \tag{16}$$

The classical motion is integrable in this limit.

For large but finite radii of curvature, one can employ semiclassical perturbation theory in R^{-1}:

$$\langle e^{i\Delta S_n/\hbar}\rangle_z = \frac{1}{L\sqrt{D^*}} \int_{-L/2}^{L/2} dz\, D(z)^{1/2} e^{-i2nk(E)[D^* - D(z)]}. \tag{17}$$

Ignoring the $1/R$-dependence of the prefactor, one finds

$$\langle e^{i\Delta S_n/\hbar}\rangle_z = \frac{C(\sqrt{nk(E)L^2/R\pi}) + iS(\sqrt{nk(E)L^2/R\pi})}{\sqrt{nk(E)L^2/R\pi}}, \tag{18}$$

where C and S are Fresnel integrals. This leads to a DOS

$$\delta g_{\rm pert}(E) = \frac{2mD^*}{\pi\hbar^2 k_E} \sum_{n=1}^{\infty} \frac{\mathcal{C}\left(2nk_E D^* - \frac{\pi}{4}, \sqrt{\frac{nk_E L^2}{\pi R}}\right)}{n\sqrt{D^*/R}}, \tag{19}$$

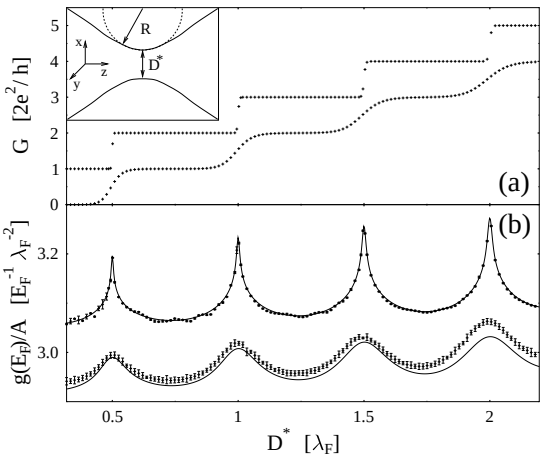

Fig. 5. (**a**) Conductance G and (**b**) DOS $g(E_F)$ for 2D nanocontacts with $\alpha \approx 5$ versus the contact diameter D^*. g is normalized to the area A of the region. Solid curves: semiclassical results based on the interpolation formula; crosses with error bars: numerical results obtained by a recursive Green's function method [24]. Lower curves in (**a**) and (**b**): $R \approx \lambda_F$; upper curves (offset vertically): $R \approx 170\lambda_F$

where we have defined the function

$$\mathcal{C}(x,y) \equiv \cos(x)\mathrm{C}(y) - \sin(x)\mathrm{S}(y). \tag{20}$$

The Gutzwiller formula (15) may be expanded in a Taylor series around $R = 0$, while the perturbation formula (19) gives a Laurent series around $R = \infty$. Combining the two, an interpolation formula valid for arbitrary R can be constructed [10]:

$$\delta g_{\mathrm{int}}(E) = \frac{\sqrt{8}mD^*}{\pi\hbar^2 k_E} \sum_{n=1}^{\infty} \frac{\mathcal{C}\left(2nk_E D^* - \frac{\pi}{4}, \sqrt{\frac{nk_E L^2}{\pi R}}\right)}{|\sinh(n\chi)|}. \tag{21}$$

The crossover from integrable to chaotic behavior in Eq. (21) is controlled by the dimensionless parameter

$$\alpha(E) = L/\sqrt{\lambda_E R}, \tag{22}$$

where $\lambda_E = 2\pi/k_E$ is the de Broglie wavelength of an electron of energy E. We refer to α as the quantum chaos parameter: for $\alpha \ll 1$ the DOS is indistinguishable from that of an integrable system, while for $\alpha \gg 1$, the DOS is that of a chaotic system.

In Fig. 5, the DOS calculated from Eq. (21) plus the 2D Weyl term is compared to the result of a numerical solution of the Schrödinger equation. Remarkably, the semiclassical result is seen to be quantitatively accurate even in the extreme quantum limit $D^* \sim \lambda_F$, $R \sim \lambda_F$.

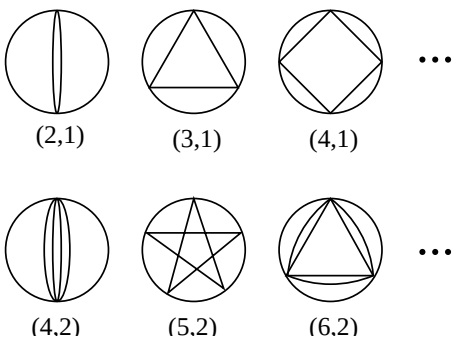

Fig. 6. Periodic orbits of an electron in the narrowest cross-section of the neck, labeled (v, w), where v is the number of vertices and w the winding number. The length of an orbit is $L_{vw} = vD^* \sin\phi_{vw}$, where $\phi_{vw} = \pi w/v$ is the angle of incidence at a vertex

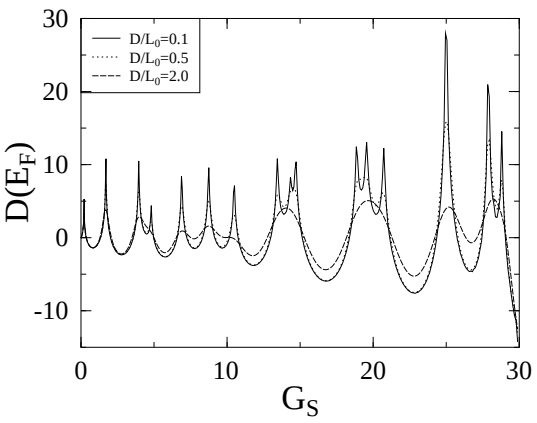

Fig. 7. DOS at the Fermi energy for axially symmetric 3D nanowires of parabolic shape versus the Sharvin conductance G_S. The different curves represent contacts with various ratios of D/L_0 (indicated in the inset), where D is the asymptotic diameter of the constriction and L_0 its initial length

4.2 3D nanowire with axial symmetry

For an axially-symmetric three-dimensional nanocontact, the periodic orbits (see Fig. 6) occur in one-dimensional families which fit into the narrowest cross-section of the contact. This problem was first investigated by Balian and Bloch [4], who derived the axially-symmetric analogue of Eq. (15). We can follow the procedure outlined in Sec. 4.1 to derive an interpolation formula describing the crossover from a long nanowire ($f = 2$) to a short nanocontact ($f = 1$) [10]:

$$\delta g(E) = \frac{m}{\hbar^2} \sum_{w=1}^{\infty} \sum_{v=2w}^{\infty} \frac{f_{vw} L_{vw}^{3/2} \mathcal{C}\left(k_E L_{vw} - 3v\pi/2, \alpha(E)\sqrt{v \sin\phi_{vw}}\right)}{v^2 |\sinh(v\chi_{vw}/2)| \sqrt{\pi k_E}}, \quad (23)$$

where $f_{vw} = 1 + \theta(v - 2w)$ counts the discrete symmetry of the orbit under time-reversal, the Lyapunov exponent χ_{vw} is given by

$$e^{\chi_{vw}} = 1 + \frac{L_{vw} \sin\phi_{vw}}{vR} + \sqrt{\left(1 + \frac{L_{vw} \sin\phi_{vw}}{vR}\right)^2 - 1}, \quad (24)$$

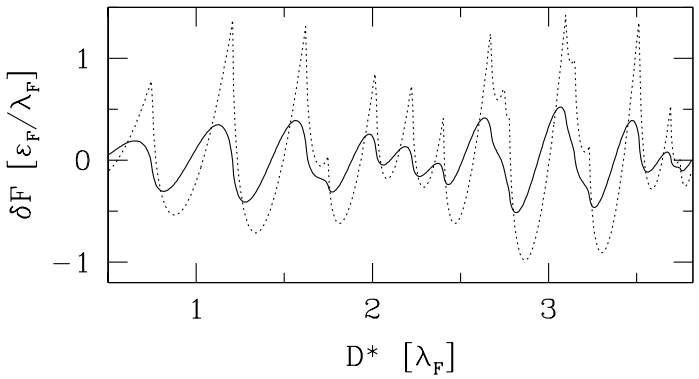

Fig. 8. Force oscillations δF versus the minimum contact diameter D^*: dashed curve: $\lim_{\alpha\to 0}\{\delta F\}$; solid curve: $\lim_{\alpha\to\infty}\{\alpha\delta F\}$. The result for $\alpha \gg 1$ is consistent with the WKB calculation shown in Fig. 3, while the result for $\alpha \to 0$ (integrable limit) agrees with the result [9] for a straight wire

and the remaining terms are defined in the caption of Fig. 6. Eq. (23) is plotted in Fig. 7. Note the rounding of the peaks in the DOS in short contacts.

5 Universal force oscillations

The characteristic amplitude of the sawtooth structure in the cohesive force of a gold nanocontact was found to be of order 1nN, independent of the contact area or shape [14,15]. To what extent is the amplitude of the force oscillations *universal*? To calculate the force from Eq. (2), we need to make some assumptions regarding how the shape of the contact scales under elongation. First, we assume that the deformation occurs primarily in the thinnest section, which implies $D^{*2}L \approx$ const. Second, we assume that $R \propto L^2$, which implies $\alpha = L/\sqrt{\lambda_F R} \approx$ const. Inserting Eq. (23) into Eq. (2), and taking the derivative, we find [10]:

$$\delta F \underset{\alpha\gg 1}{\simeq} -\frac{\varepsilon_F}{L}\sum_{w=1}^{\infty}\sum_{v=2w}^{\infty}\sqrt{\frac{L_{vw}}{\lambda_F}}\frac{f_{vw}\sin(k_F L_{vw} - 3v\pi/2 + \pi/4)}{v^2\sinh(v\chi_{vw}/2)}, \tag{25}$$

$$\delta F \underset{\alpha\ll 1}{\simeq} -\frac{2\varepsilon_F}{\lambda_F}\sum_{w=1}^{\infty}\sum_{v=2w}^{\infty}\frac{f_{vw}}{v^2}\sin(k_F L_{vw} - 3v\pi/2). \tag{26}$$

$$\mathrm{rms}\,\delta F = \frac{\varepsilon_F}{\lambda_F}\times\begin{cases} 0.58621, & \alpha \ll 1, \\ 0.36208\,\alpha^{-1}, & \alpha \gg 1. \end{cases} \tag{27}$$

From Figs. 1 and 2, one sees that $\alpha < 1$ for a realistic geometry, implying that indeed $\mathrm{rms}\,\delta F \sim \varepsilon_F/\lambda_F$.

6 Quantum suppression of the Rayleigh instability

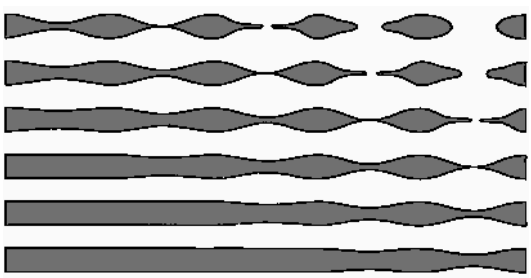

Fig. 9. Artist's conception of a propagating Rayleigh instability, from Ref. [28]

A cylindrical body longer than its circumference is unstable to breakup under surface tension [26,27] (see Fig. 9). How then to explain the durability of long gold nanowires [c.f. Fig. 2(b)], the thinnest of which have been shown [22] to be almost perfectly cylindrical in shape? Let us calculate the quantum corrections [12] to the classical stability analysis. Classically, only axially-symmetric deformations lead to instabilities. Any such deformation of a cylinder may be written as a Fourier series

$$R(z) = R_0 + \int_{-\infty}^{\infty} dq\, b(q) e^{iqz}, \tag{28}$$

where $R(z)$ is the radius of the cylinder at z and R_0 the unperturbed radius. The constant volume constraint leads to the condition

$$b(0) = -\frac{1}{R_0} \int_0^{\infty} dq\, |b(q)|^2. \tag{29}$$

In the Weyl approximation, the energy cost of the deformation is

$$\begin{aligned} \Delta\bar{\Omega}/\varepsilon_F = & \left(-\frac{8}{15} k_F^3 R_0 + \frac{\pi}{4} k_F^2 \right) b(0) \\ & + \int_0^{\infty} dq \left[-\frac{8k_F^3}{15} + \left(\frac{\pi k_F^2 R_0}{4} - \frac{8k_F}{9} \right) q^2 \right] |b(q)|^2. \end{aligned} \tag{30}$$

For the unperturbed cylinder, Eq. (8) yields

$$\delta g(E) = \frac{mL}{\pi\hbar^2} \sum_{w=1}^{\infty} \sum_{v=2w}^{\infty} \frac{f_{vw} L_{vw}}{v^2} \cos(k_E L_{vw} - 3v\pi/2). \tag{31}$$

The effect of the deformation may be treated with semiclassical perturbation theory:

$$\langle e^{i\Delta S_{vw}(z)/\hbar} \rangle_z = \frac{1}{LR_0} \int_0^L dz\, R(z)\, e^{i\Delta S_{vw}(z)/\hbar}, \tag{32}$$

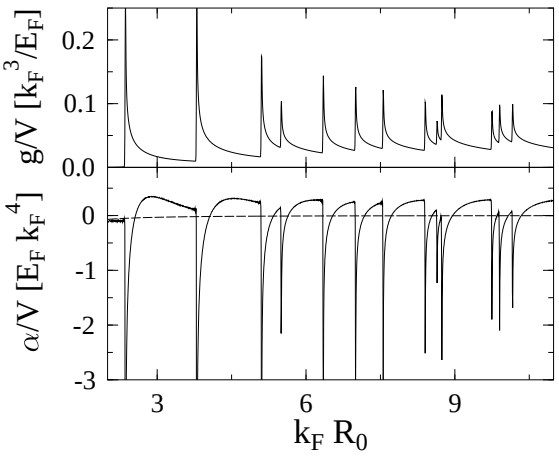

Fig. 10. Density of states $g(E_F)$ of a cylindrical wire (upper diagram) and stability coefficient α (lower diagram) versus the radius R_0 of the unperturbed wire. The wavevector of the perturbation is $qR_0 = 1$. Dashed curve: Weyl contribution to α

where

$$\frac{\Delta S_{vw}(z)}{\hbar} = 2v \sin\phi_{vw} k_E \int_{-\infty}^{\infty} dq\, b(q) e^{iqz}. \tag{33}$$

Expanding δg up to second order in $b(q)$ gives

$$\Delta\{\delta g(E)\} = \frac{4m}{\hbar^2} \sum_{w=1}^{\infty} \sum_{v=2w}^{\infty} \frac{f_{vw} \sin\phi_{vw}}{v} \left[b(0)(\cos\theta_{vw} - k_E L_{vw} \sin\theta_{vw}) \right.$$
$$\left. - \frac{k_E L_{vw}}{R_0} \int_0^{\infty} dq\, |b(q)|^2 \left(\sin\theta_{vw} + \frac{k_E L_{vw}}{2} \cos\theta_{vw} \right) \right], \tag{34}$$

where $\theta_{vw}(E) = k_E L_{vw} - 3v\pi/2$.

Combining Eqs. (30) and (34), and using the constraint (29), one finds that the change of the DOS is of second order in b, and contributions with different q decouple. The energy integral (2) yields

$$\Omega[b] = \Omega[0] + \int_0^{\infty} dq\, \alpha(q) |b(q)|^2 + \mathcal{O}(b^3), \tag{35}$$

where the stability coefficient $\alpha(q)$ depends implicitly on R_0 and temperature. If $\alpha(q)$ is negative for any value of q, then Ω decreases under the deformation and the wire is unstable.

Fig. 10 shows the stability coefficient and DOS at the classical stability threshold $qR_0 = 1$ as a function of R_0. The quantum correction destabilizes the wire where the DOS is sharply peaked; but what is more surprising, it *stabilizes* the wire in the intervening intervals. With these results, we can construct a stability diagram for the wire. For a given temperature, the stability

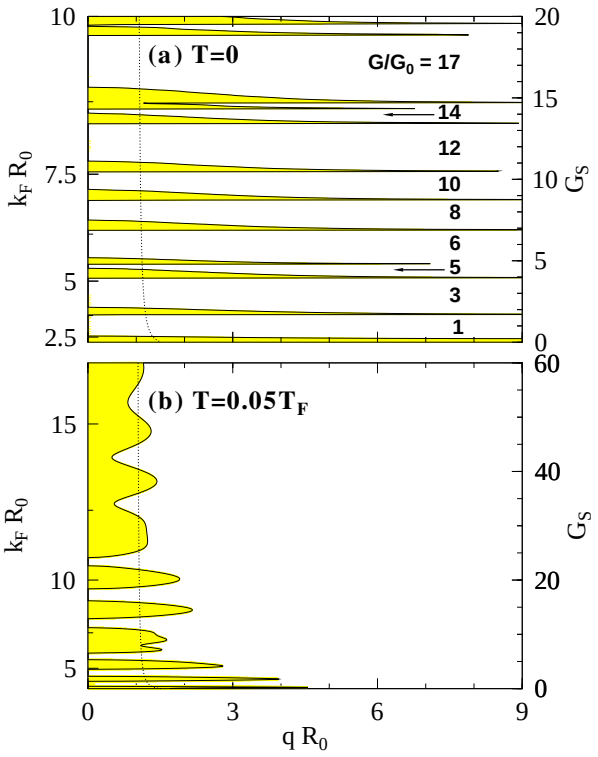

Fig. 11. Stability diagram for cylindrical nanowires at two different temperatures. White areas are stable, grey unstable to small perturbations. The quantized electrical conductance values G of the stable configurations are indicated by bold numerals in (**a**), with $G_0 = 2e^2/h$. Right vertical axis: corrected Sharvin conductance G_S. Dotted curve: stability criterion in the Weyl approximation

problem is now determined by two dimensionless parameters: qR_0 and $k_F R_0$. In Fig. 11, regions of instability, where $\alpha(q) < 0$, are shaded grey, while stable regions are shown in white. Note that many of the white regions of stability persist all the way down to $q = 0$, indicating that an infinitely long wire is a true metastable state if its radius lies in one of the windows of stability. The quantized conductance values of the stable cylindrical configurations are indicated by bold numerals in Fig. 11(a). Our stability analysis is consistent with recent experimental results for alkali metal nanowires [21].

Acknowledgments

CAS is indebted to Dionys Baeriswyl and Jérôme Bürki for their contributions to the early phase of this work, and to Raymond Goldstein for his insights on the quantum Rayleigh problem. CAS was supported by NSF Grant DMR0072703. FK and HG were supported by Grant SFB 276 of the Deutsche Forschungsgemeinschaft. This research was supported by an award from Research Corporation.

References

1. M. C. Gutzwiller, J. Math. Phys. **12**, 343 (1971)
2. M. C. Gutzwiller, *Chaos in Classical and Quantum Mechanics* (Springer, New York, 1990)
3. M. Brack and R. K. Bhaduri, *Semiclassical Physics*. (Addison-Wesley, Reading, MA, 1997)
4. R. Balian and C. Bloch, Ann. Phys. NY **69**, 76 (1972).
5. S. C. Creagh and R. G. Littlejohn, Phys. Rev. A **44**, 836 (1991)
6. D. Ullmo, M. Grinberg, and S. Tomsovic, Phys. Rev. E **54**, 136 (1996)
7. S. C. Creagh, Ann. Phys. (N.Y.) **248**, 60 (1996)
8. P. Meier, M. Brack, and S. C. Creagh, Z. Phys. D **41**, 281 (1997); M. Brack, Adv. Solid State Phys. (this volume)
9. C. Höppler and W. Zwerger, Phys. Rev. B **59**, R7849 (1999)
10. C. A. Stafford, F. Kassubek, J. Bürki, and H. Grabert, Phys. Rev. Lett. **83**, 4836 (1999)
11. F. Kassubek, C. A. Stafford, and H. Grabert, Physica B **280**, 438 (2000)
12. F. Kassubek, C. A. Stafford, H. Grabert, and R. E. Goldstein, Nonlinearity **14**, 167 (2001)
13. For a review, see *Nanowires*, P. A. Serena and N. Garcia eds. (Kluwer Academic, Dordrecht, 1997)
14. G. Rubio, N. Agraït, and S. Vieira, Phys. Rev. Lett. **76**, 2302 (1996)
15. A. Stalder and U. Dürig, Appl. Phys. Lett. **68**, 637 (1996); U. Dürig, in Ref. [13]
16. Y. Kondo and K. Takayanagi, Phys. Rev. Lett. **79**, 3455 (1997)
17. J. L. Costa-Krämer *et al.*, Phys. Rev. B **55**, 5416 (1997)
18. E. Scheer, N. Agraït, J. C. Cuevas, A. Levy Yeyati, B. Ludoph, A. Martín-Rodero, G. Rubio Bollinger, J. M. van Ruitenbeek, and C. Urbina, Nature **394**, 154 (1998)
19. H. Ohnishi, Y. Kondo, and K. Takayanagi, Nature **395**, 780 (1999)
20. A. I. Yanson *et al.*, Nature **395**, 783 (1999)
21. A. I. Yanson, I. K. Yanson, and J. M. van Ruitenbeek, Nature **400**, 144 (1999); Phys. Rev. Lett. **84**, 5832 (2000)
22. Y. Kondo and K. Takayanagi, Science **289**, 606 (2000)
23. For a review, see C. W. J. Beenakker and H. van Houten, in *Solid State Physics: Advances in Research and Applications*, H. Ehrenreich and D. Turnbull eds. (Academic Press, New York, 1991) Vol. 44, p. 1
24. J. Bürki, C. A. Stafford, X. Zotos, and D. Baeriswyl, Phys. Rev. B **60**, 5000 (1999)
25. C. A. Stafford, D. Baeriswyl, and J. Bürki, Phys. Rev. Lett. **79**, 2863 (1997)
26. J. Plateau, *Statique experimentale et theorique des liquides soumis aux seules forces moleculaires*, (Gautier-Villars, Paris, 1873)
27. S. Chandrasekhar, *Hydrodynamic and Hydromagnetic Stability* (Dover, New York, 1981) pp 515-74
28. T. R. Powers and R. E. Goldstein, Phys. Rev. Lett. **78**, 2555 (1997)
29. F. Kassubek, C. A. Stafford, and H. Grabert, Phys. Rev. B **59**, 7560 (1999)
30. R. Landauer, IBM J. Res. Dev. **1**, 223 (1957); Philos. Mag. **21**, 863 (1970)
31. D. S. Fisher and P. A. Lee, Phys. Rev. B **23**, 6851 (1981)
32. J. A. Torres, J. I. Pascual, and J. J. Sáenz, Phys. Rev. B **49**, 16581 (1994)
33. R. Dashen, S.-K. Ma, and H. J. Bernstein, Phys. Rev. **187**, 345 (1969)